Three distinct *Atoh1* enhancers cooperate for sound receptor hair cell development

Zhengnan Luo[a,b,1] , Yi Du[b,c,1] , Shuting Li[a,b] , He Zhang[a,b], Muya Shu[b,c], Di Zhang[a,b] , Shunji He[a] , Guangqin Wang[a,b] , Falong Lu[b,c,2], and Zhiyong Liu[a,b,d,2]

Cochlear hair cells (HCs) in the inner ear are responsible for sound detection. For HC fate specification, the master transcription factor Atoh1 is both necessary and sufficient. *Atoh1* expression is dynamic and tightly regulated during development, but the *cis*-regulatory elements mediating this regulation remain unresolved. Unexpectedly, we found that deleting the only recognized *Atoh1* enhancer, defined here as Eh1, failed to impair HC development. By using the assay for transposase-accessible chromatin with high-throughput sequencing (ATAC-seq), we discovered two additional *Atoh1* enhancers: Eh2 and Eh3. Notably, Eh2 deletion was sufficient for impairing HC development, and concurrent deletion of Eh1 and Eh2 or all three enhancers resulted in nearly complete absence of HCs. Lastly, we showed that Atoh1 binds to all three enhancers, consistent with its autoregulatory function. Our findings reveal that the cooperative action of three distinct enhancers underpins effective *Atoh1* regulation during HC development, indicating potential therapeutic approaches for HC regeneration.

Atoh1 | hair cell | cochlea | inner ear | enhancer

Sound information is detected by cochlear hair cells (HCs) located in the inner ear auditory epithelium, which is also referred to as the organ of Corti (OC) (1, 2). Two cochlear HC subtypes are recognized, the inner hair cells (IHCs) and outer hair cells (OHCs), and the OC harbors one row of IHCs and three rows of OHCs (3). IHCs and OHCs share several pan-HC markers, such as *Myo6*, *Myo7a*, *Gfi1*, *Pou4f3*, and *Rbm24* (4–7), but they also have their own unique markers. *Otoferlin* and *Slc17a8* (*vGlut3*) are specifically expressed in IHCs (8–10), and *Slc26a5* (*Prestin*) and *Bcl11b* are exclusively expressed in OHCs (11–13). Near the cochlear HCs are supporting cells (SCs) expressing *Sox2* and *Sox10* (7, 14, 15).

Atoh1, a bHLH-family transcription factor (TF), is both necessary and sufficient for cochlear HC development: no HCs develop in $Atoh1^{-/-}$ cochleae (16), and supernumerary HCs form upon ectopic *Atoh1* expression (17, 18). The ability of Atoh1 to generate HCs has made it the focus and key target in preclinical HC regeneration studies (19–22). Atoh1 is initially expressed at low levels in cochlear prosensory progenitors but markedly increased in nascent HCs (23–25). However, how *Atoh1* expression is temporally and spatially regulated remains poorly understood. Enhancers are crucial *cis*-regulatory elements that can be located upstream, downstream, or within the introns of a gene (26). The expression of a gene can be controlled by multiple enhancers, and each enhancer may contribute to gene expression in a specific cell type or at a particular developmental stage (27). Previous studies have suggested that an ~1.5-kb fragment, located ~2.1 kb downstream of *Atoh1* (28–30), serves as an *Atoh1* enhancer; we define this as enhancer 1 (Eh1), in this study (29, 31). Moreover, Eh1 represents one of the presumptive sequences necessary for *Atoh1* autoregulation (3, 28, 32). However, whether Eh1 is necessary for *Atoh1* expression and HC development in vivo has remained unclear.

Here, we performed assay for transposase-accessible chromatin with high-throughput sequencing (ATAC-seq) analysis on neonatal cochlear HCs, which revealed, in addition to Eh1, two previously unknown cochlear HC *Atoh1* enhancers: enhancer 2 (Eh2) and enhancer 3 (Eh3). Eh2 and Eh3 are sufficient to drive enhanced green fluorescent protein (EGFP) reporter expression selectively in cochlear HCs. We generated mice in which Eh1, Eh2, or Eh3 was deleted. Contrary to the longstanding expectation, we observed no cochlear HC phenotypes in the $Eh1^{-/-}$ mice, and we instead found that deletion of Eh2 alone was adequate for impairing HC development. Moreover, no phenotypes related to cochlear HC development were evident in $Eh3^{-/-}$ mice. Notably, HCs were nearly absent from $Eh1^{-/-};Eh2^{-/-}$ double mutants and $Eh1^{-/-};Eh2^{-/-};Eh3^{-/-}$ triple mutants. Collectively, our in vivo studies provide evidence that 1) Eh2, but not Eh1 or Eh3, is most critical for *Atoh1* expression in cochlear HCs and 2) the absence of both

Significance

The expression of *Atoh1*, a gene essential for cochlear hair cell (HC) development, is tightly regulated. A previously identified *Atoh1* enhancer is considered vital for regulating *Atoh1* expression, but direct evidence is lacking. It also remains unknown whether additional enhancers exist and play critical roles in controlling *Atoh1* expression. This study makes four contributions: 1) genomewide open chromatin regions of neonatal cochlear HCs are revealed, 2) two previously unknown *Atoh1* enhancers are identified and validated, 3) individual and synergistic functions of the three enhancers are uncovered using seven mutant models, and 4) Atoh1 protein is shown to bind to all three *Atoh1* enhancers. These provide insights into the molecular mechanisms underlying *Atoh1* expression and subsequent HC development.

[1]Z. Luo and Y.D. contributed equally to the work.

[2]To whom correspondence may be addressed. Email: fllu@genetics.ac.cn or zhiyongliu@ion.ac.cn.

Eh1 and Eh2, or of all three enhancers, almost completely abolishes cochlear HC development, suggesting that the enhancers collaborate to orchestrate *Atoh1* expression. Furthermore, Atoh1 protein binds directly to Eh1, Eh2, and Eh3. Our study provides insights into the longstanding question of how *Atoh1* expression is tightly regulated during cochlear HC development, and these insights are directly relevant to studies on HC regeneration for hearing restoration in hearing-impaired patients.

Results

Eh1 Is Necessary for Development of Cerebellum but Not Cochlear HCs.

We first determined the necessity of Eh1 in cochlear HC development. Several lines of evidence suggest that Eh1 is involved in cochlear HC development (28, 33–36), but direct in vivo genetic evidence indicating that Eh1 ablation abolishes cochlear HC development is lacking. Thus, we generated Eh1$^{+/-}$ mice, wherein an ~2-kb segment covering Eh1 was deleted between the single guide RNA (sgRNA)-1 and the sgRNA-2 sites (Fig. 1 *A* and *B*, and *SI Appendix*, Fig. S1 *A–C*). In contrast to *Atoh1*$^{-/-}$ mice, which die immediately after birth (16), Eh1$^{-/-}$ mutants survived until ~postnatal day 35 (P35). Unexpectedly, labeling for the pan-HC marker Myo6 revealed that as in wild-type (WT) Eh1$^{+/+}$ mice ($n = 3$), cochlear HC development appeared normal in the basal or middle turn of Eh1$^{-/-}$ mice ($n = 3$) at embryonic day 16.5 (E16.5) (Fig. 1 *C–D'*). Moreover, colabeling for the IHC marker vGlut3 and OHC marker Prestin showed that cochlear HC development was also similar in control Eh1$^{+/+}$ ($n = 3$) and Eh1$^{-/-}$ ($n = 3$) mice in all turns at P30 (Fig. 1 *E–F'*). Thus, our results indicate that absence of Eh1 alone affects neither early HC specification nor late HC differentiation. Accordingly, auditory brainstem response (ABR) measurements revealed no significant difference in hearing thresholds between Eh1$^{+/+}$ ($n = 3$) and Eh1$^{-/-}$ ($n = 3$) mice (Fig. 1*G*).

Notably, Eh1$^{-/-}$ mice ($n = 3$) displayed balance impairment, but vestibular HC development was not different between Eh1$^{+/+}$ ($n = 3$) and Eh1$^{-/-}$ ($n = 3$) mice (*SI Appendix*, Fig. S1 *D–G*), which suggested that the balance impairment was not because of HC loss in vestibular organs. The balance-control defect was instead at least partly due to aberrant cerebellum development (Fig. 1 *H–I*). Thus, Eh1 functions as an essential *Atoh1* enhancer during cerebellum development, because *Atoh1* is also highly expressed in proliferating cerebellar granule neuron precursors (GNPs) in the external granule layer of the mouse cerebellum within the first two postnatal weeks (37, 38). Collectively, our in vivo genetic data indicate that the Eh1 enhancer of *Atoh1* is not essential for cochlear HC development. These results were unexpected considering the longstanding assumption regarding the crucial role of Eh1 in *Atoh1* expression and HC development and further led us to search for additional *Atoh1* enhancers.

Generating the *Atoh1*-3*V5-P2A-Tdtomato/$^+$ Mouse Strain for Neonatal Cochlear HC Sorting and ATAC-Seq Analysis.

To search for previously unreported *Atoh1* enhancers, we used neonatal (P1) cochlear HCs to perform ATAC-seq, a widely used approach to identify open chromatin regions where enhancers are likely located (33, 39). The optimal model for this assay is a mouse strain in which only HCs are labeled with a bright fluorescent reporter protein at P1 for use in fluorescence-activated cell sorting (FACS). We initially used *Atoh1*-EGFP/$^+$ mice, wherein EGFP is fused to the Atoh1 C terminus (40), but failed to obtain pure cochlear
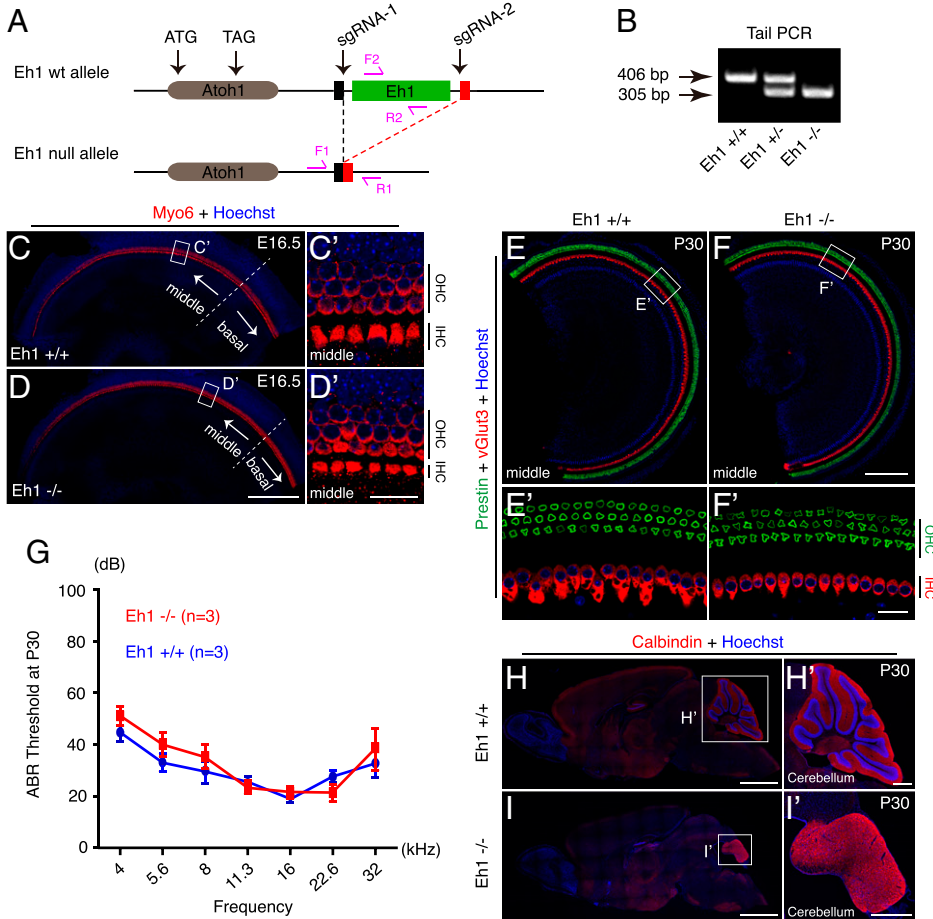

Fig. 1. Development of cerebellum, but not cochlea, is aberrant in the absence of Eh1. (*A*) Illustration depicting deletion of Eh1, which lies between the sgRNA-1 and the sgRNA-2 sites. (*B*) Gel image of tail-DNA PCR. WT allele band: 406 bp; Eh1 null-allele band: 305 bp. (*C–D'*) Labeling for pan-HC marker Myo6 in Eh1$^{+/+}$ (*C–C'*) and Eh1$^{-/-}$ (*D–D'*) cochleae at E16.5. Boxed areas in *C* and *D* are magnified in *C'* and *D'*. (*E–F'*) Double labeling for OHC marker Prestin and IHC marker vGlut3 in whole-mount cochlear samples from Eh1$^{+/+}$ (*E* and *E'*) and Eh1$^{-/-}$ (*F* and *F'*) mice at P30. Boxed areas in *E* and *F* are magnified in *E'* and *F'*. (*G*) ABR measurements from Eh1$^{+/+}$ (blue line) and Eh1$^{-/-}$ (red line) mice. No significant difference was detected at any tested frequency in terms of hearing threshold; Student's *t* test was used for statistical analysis. (*H–I'*) Immunolabeling for Calbindin in cryosectioned cerebellum tissue. Cerebellum was considerably smaller in Eh1$^{-/-}$ mice (*I–I'*) than in control Eh1$^{+/+}$ mice (*H* and *H'*). Boxed areas in *H* and *I* are magnified in *H'* and *I'*. Scale bars: 2 mm (*H* and *I*), 500 μm (*H'* and *I'*), 200 μm (*D* and *F*), 20 μm (*D'* and *F'*). Error bars are SEM.
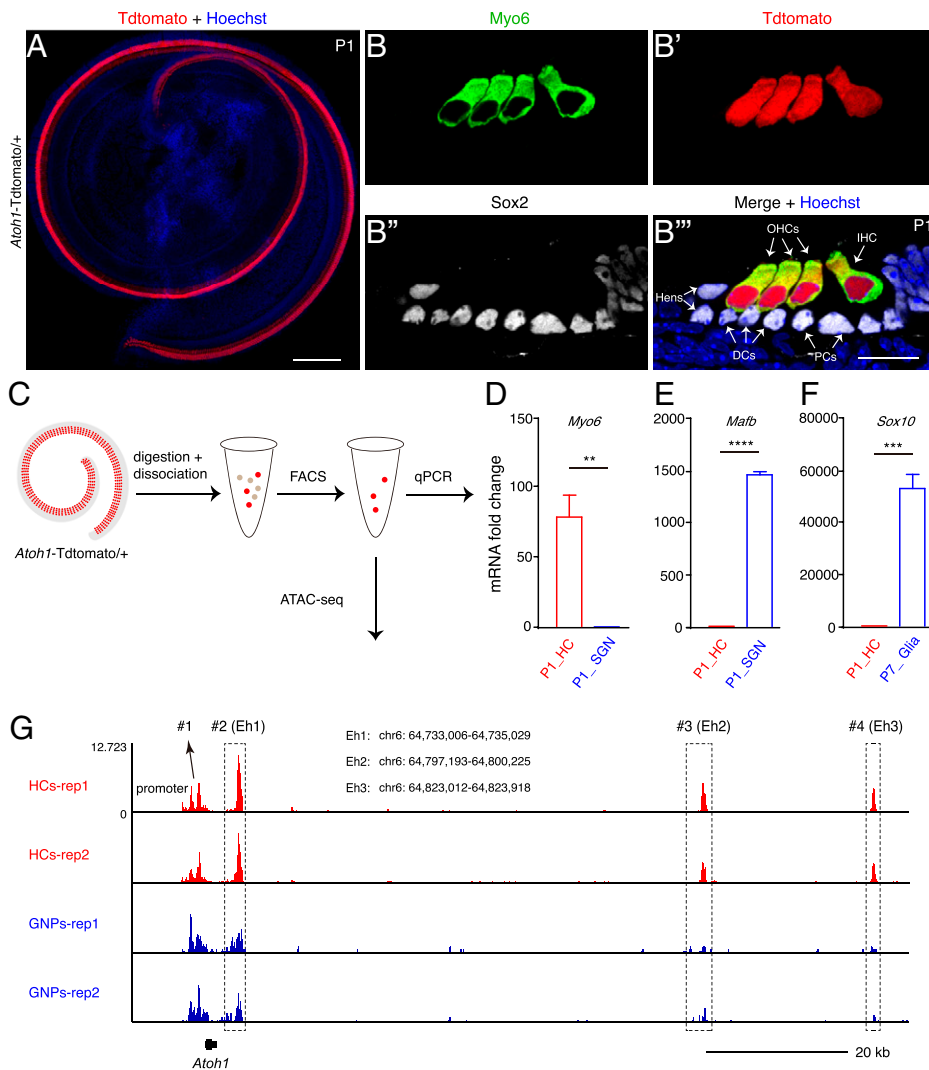
Fig. 2. ATAC-seq of cochlear HCs sorted from *Atoh1*-Tdtomato/⁺ mice at P1. (*A–B‴*) Whole-mount (*A*) and cryosection (*B–B‴*) analyses of cochleae of *Atoh1*-Tdtomato/⁺ mice at P1. Endogenous Tdtomato is highly expressed in all cochlear turns (*A*). (*B–B‴*) Triple labeling for Myo6 (HC marker), Sox2 (SC marker), and Tdtomato. Tdtomato was exclusively detected in HCs and not detected in any SCs, which include Pillar cells (PCs), Deiters' cells (DCs), and Hensen's cells (Hens). (*C*) Illustration of how pure cochlear HCs at P1 are obtained using FACS. (*D–F*) Confirmation of HC purity through qPCR analysis of HC gene *Myo6* (*D*), SGN gene *Mafb* (*E*), and glial/SC gene *Sox10* (*F*): *Myo6* was significantly enriched and *Mafb* and *Sox10* were drastically depleted in sorted HCs. Data are presented as means ± SEM; **$P < 0.01$, ***$P < 0.001$, ****$P < 0.0001$ (Student's *t* test). (*G*) Integrative genomics viewer (IGV) visualization of ATAC-seq peaks in *Atoh1* locus. Four peaks are present: 1, Atoh1 promoter; 2, Eh1; and 3 and 4, Eh2 and Eh3, the two enhancers newly identified in this study. Scale bars: 200 μm (*A*), 20 μm (*B‴*). Error bars are SEM.

HCs, partly because the EGFP signal was not adequately strong for cell sorting. Thus, we generated a knockin (KI) mouse strain, *Atoh1*-3*V5-P2A-Tdtomato/⁺ (*Atoh1*-Tdtomato/⁺), in which three V5 tags were fused to the Atoh1 C terminus and Tdtomato expression was controlled by *Atoh1* endogenous promoters/enhancers (*SI Appendix*, Fig. S2 *A–C*).

We used Southern blotting to confirm the absence of random donor-DNA insertion in the mouse genome (*SI Appendix*, Fig. S2 *D* and *E*), and we used PCR to distinguish between the WT and KI alleles (*SI Appendix*, Fig. S2*F*). Both heterozygous *Atoh1*-Tdtomato/⁺ and homozygous *Atoh1*-Tdtomato/*Atoh1*-Tdtomato mice were healthy and fertile, and the homozygous mice displayed no overt phenotypes. Although embryonic *Atoh1* expression is detected in both cochlear SCs and HCs (23, 41, 42), *Atoh1* is exclusively expressed in cochlear HCs at P1 (25, 41, 43). Accordingly, we detected bright Tdtomato fluorescence in cochlear IHCs and OHCs in all turns but not in any cochlear SCs (Fig. 2 *A–B″*). We confirmed that all Tdtomato⁺ cells were HCs, and vice versa, in cochleae at P1. Therefore, our *Atoh1*-Tdtomato/⁺ mouse line is suitable for sorting pure neonatal cochlear HCs.

ATAC-Seq Analysis of Genomewide Open Chromatin Status in Neonatal Mouse Cochlear HCs. To perform ATAC-seq, we collected Tdtomato⁺ cochlear HCs from P1 *Atoh1*-Tdtomato/⁺ mice by using FACS (Fig. 2*C*). First, we used qPCR to validate

HC purity (Fig. 2 *D–F*): In sorted HCs, the HC gene *Myo6* was enriched 79.4 ± 15.6-fold, whereas the spiral ganglion neuron (SGN) gene *Mafb* and glial/SC marker *Sox10* were depleted 1,477.0 ± 37.3- and 53,774.0 ± 6,030.0-fold, respectively (*n* = 3 replicates, each containing ∼50 HCs from two cochleae at P1). Second, we used two replicates (each containing ∼500 HCs from 18 cochleae at P1) to perform ATAC-seq, which revealed four clear peaks, 1 to 4, at the *Atoh1* locus (Fig. 2*G*). Peak 1 lies within the *Atoh1* promoter and is located upstream of 5′-untranslated region (UTR); peak 2 corresponds to Eh1 (Fig. 1). We also sorted Tdtomato⁺ GNPs from the cerebellum at P7, and these cells also expressed Pax6 and Atoh1 (V5) (*SI Appendix*, Fig. S3 *A–B″*). ATAC-seq performed on two GNP replicates (each containing ∼500 GNPs from one cerebellum) revealed that, intriguingly, peak 2 was present in but peaks 3 and 4 were absent from the cerebellar GNP ATAC-seq data (Fig. 2*G*). This raises the possibility that peaks 3 and 4 represent cochlear HC-specific *cis*-regulatory regions.

We also identified genomic regions that are open only in HCs or GNPs or open in both cell types (*SI Appendix*, Fig. S3 *C–E*). First, ATAC-seq peaks in HC-specific genes, such as *Pou4f3*, *Gfi1*, and *Myo7a*, were captured robustly in HCs but minimally in GNPs (*SI Appendix*, Fig. S3*C*). Second, peaks in GNP-specific genes, such as *Pax6*, *Neurod1*, and *Zic4* (44), were detected robustly in GNPs but minimally in HCs (*SI Appendix*, Fig. S3*D*). Third, peaks in *Rbm24*, *Pvalb*, and *Calb1*
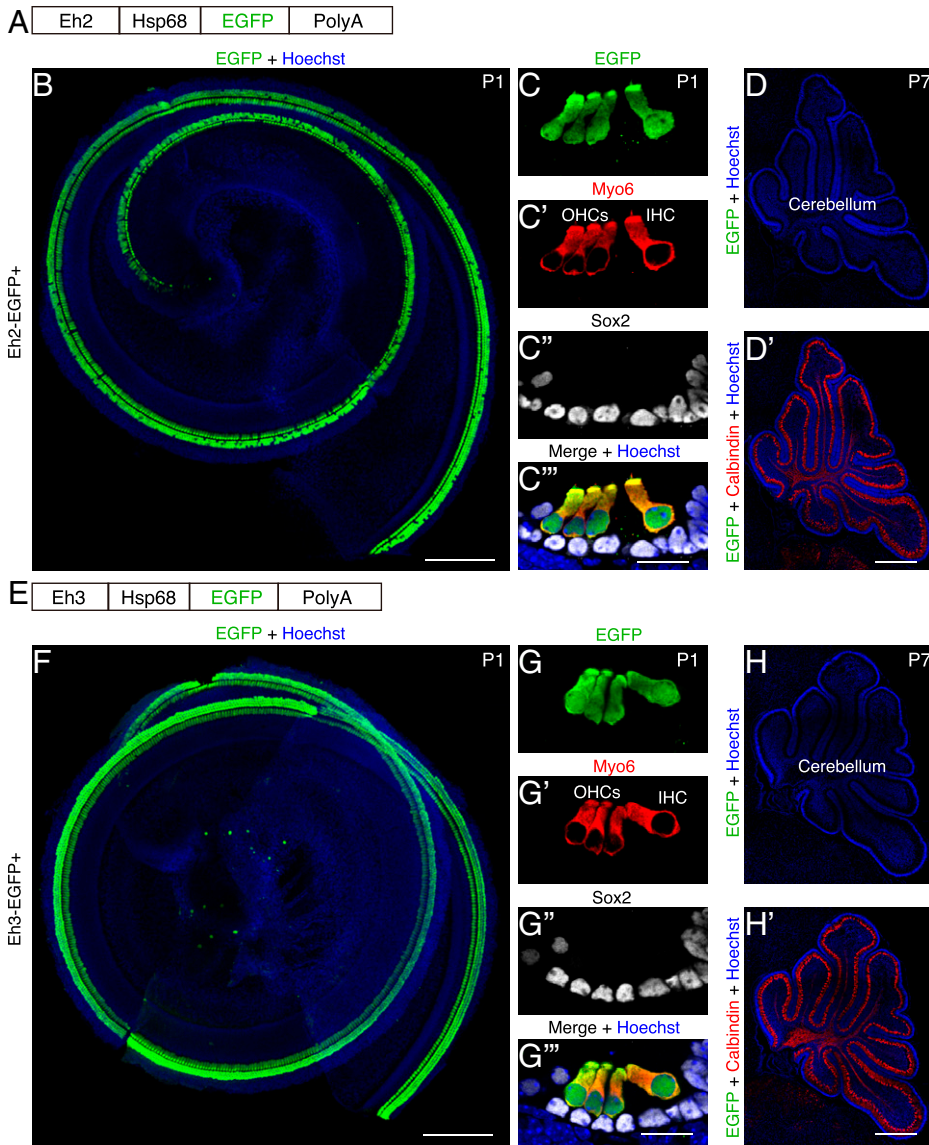
Fig. 3. Both Eh2 and Eh3 can drive HC-specific reporter-gene expression in cochleae at P1 but not in cerebellum at P7. (A) Simple illustration of the design of the Eh2-EGFP+ transgenic mouse strain; detailed information is presented in *SI Appendix*, Fig. S4 A and B. (B) EGFP labeling of a whole-mount cochlear sample from a P1 Eh2-EGFP+ mouse. EGFP was highly expressed in the majority of HCs. (C–C''') Triple labeling for EGFP (C), HC marker Myo6 (C'), and SC marker Sox2 (C'') in a cryosection cochlear sample from a P1 Eh2-EGFP+ mouse. EGFP was expressed in HCs but not SCs. (D–D') Double labeling for EGFP and Calbindin in cerebellum from a P7 Eh2-EGFP+ mouse. No EGFP+ cells were observed in the cerebellum (D). (E) Simple illustration of design of the Eh3-EGFP+ transgenic mouse strain; detailed information is presented in *SI Appendix*, Fig. S4 C and D. (F) EGFP labeling of whole-mount cochlear sample from a P1 Eh3-EGFP+ mouse. All cochlear HCs were EGFP+. (G–G''') Triple labeling for EGFP (G), Myo6 (G'), and Sox2 (G'') in a cryosection cochlear sample from a P1 Eh3-EGFP+ mouse. Again, EGFP was exclusively expressed in HCs and not detected in any SCs. (H–H') Double labeling for EGFP and Calbindin in cerebellum from a P7 Eh3-EGFP+ mouse. No EGFP+ cells were detected in the cerebellum (H). Scale bars: 500 μm (D' and H'), 200 μm (B and F), 20 μm (C''' and G'''). PolyA, polyadenylation signal sequence.

were detected in both HCs and GNPs (*SI Appendix*, Fig. S3E). These results confirmed the quality of our ATAC-seq data. In Dataset S1, we summarize all open chromatin regions in P1 cochlear HCs and P7 GNPs. Moreover, analysis of the data from a recent study (33) indicated that the epigenetic modifications of monomethylation of lysine 4 on histone H3 (H3K4me1) and histone H3 lysine 27 acetylation (H3K27ac) are present at sites corresponding to peaks 2, 3, and 4 (*SI Appendix*, Fig. S3F). The existence of H3K4me1 and H3K27ac dual modifications strongly supports the notion that they are active enhancers (45, 46). Thus, we hypothesized that our ATAC-seq peaks 3 and 4 potentially represent previously unknown *Atoh1* enhancers in cochlear HCs, and we defined them as Eh2 and Eh3, respectively (Fig. 2G and *SI Appendix*, Fig. S3F).

Eh2 and Eh3 Are Sufficient to Drive EGFP Reporter Expression Specifically in Cochlear HCs but Not in Cerebellar GNPs. To determine whether Eh2 and Eh3 are bona fide *Atoh1* enhancers, we generated transgenic mice to test whether each element could, together with a minimal promoter from mouse heat shock protein 68 kDa (hsp68) (47, 48), drive EGFP expression specifically in cochlear HCs in vivo. According to our ATAC-seq data, Eh2 spans ~3 kb of DNA, which includes a clear peak (1,027 bp) and

a long tail sequence (~2 kb) (*SI Appendix*, Fig. S4A). We selected the peak DNA fragment (1,027 bp) to generate Eh2-hsp68-EGFP+ (Eh2-EGFP+) transgenic mice, wherein EGFP expression is controlled by hsp68 and the 1,027-bp Eh2 fragment (Fig. 3A and *SI Appendix*, Fig. S4B). Whole-mount analysis revealed that numerous EGFP+ cells were present in Eh2-EGFP+ cochleae at P1 (*n* = 3) (Fig. 3B). Furthermore, triple labeling for Myo6, Sox2 (SC marker), and EGFP showed that EGFP+ cells in all turns were Myo6+/Sox2− cochlear IHCs and OHCs (Fig. 3 C–C''). By contrast, EGFP was not detected in cochlear SCs that were Sox2+/Myo6− (Fig. 3 C–C''). Notably, EGFP+ cells were absent from the cerebellum of Eh2-EGFP+ mice at P7 (Fig. 3 D and D').

For studying Eh3, we selected the 761-bp DNA fragment covering the Eh3 peak (*SI Appendix*, Fig. S4C) to generate Eh3-hsp68-EGFP+ (Eh3-EGFP+) transgenic mice (Fig. 3E and *SI Appendix*, Fig. S4D). As in Eh2-EGFP+ mice, EGFP was highly expressed in almost all IHCs and OHCs, but not in SCs, in Eh3-EGFP+ mice at P1 (Fig. 3 F–G''). EGFP+ cells were also sporadically detected in neural regions of cochlear ducts (*SI Appendix*, Fig. S4E), but triple labeling for EGFP, neuron marker Tuj1, and glial marker Sox10 showed that the EGFP+ cells were neither SGNs nor glial cells (arrows in *SI Appendix*, Fig. S4 F–F'''). Again, as in Eh2-EGFP+ mice

(Fig. 3 *D* and *D'*), EGFP⁺ cells were absent from the cerebellum of Eh3-EGFP⁺ mice at P7 (Fig. 3 *H* and *H'*). Together, our results indicate that both Eh2 and Eh3 are functional *Atoh1* enhancers and are active in neonatal cochlear HCs but not cerebellar GNPs, thus mimicking the reported expression pattern of endogenous *Atoh1* in cochleae at neonatal ages (24, 41, 43, 49).

Loss of Eh2 Alone Is Sufficient to Cause Mild Phenotypes of Cochlear HC Development and Hearing Impairment at High Frequency. We next determined whether Eh2 and Eh3 are necessary for cochlear HC development. First, we used the CRISPR-Cas9 approach to generate Eh2$^{+/-}$ mice in which an ~2.5-kb fragment between the sgRNA-3 and the sgRNA-4 sites was deleted (Fig. 4 *A* and *B*, and *SI Appendix*, Fig. S5). Whereas cochleae from WT control Eh2$^{+/+}$ littermates contained three

regularly aligned rows of Bcl11b⁺ OHCs (13) (Fig. 4 *C–D'*), Eh2$^{-/-}$ cochleae at P1 contained a missing or discontinuous third row of OHCs on the lateral side (Fig. 4*E*). Notably, OHC loss occurred only in the basal turn (yellow asterisks in Fig. 4 *F* and *F'*). Furthermore, labeling for the OHC marker Prestin revealed that relative to Eh2$^{+/+}$ cochleae (Fig. 4*G*), Eh2$^{-/-}$ cochleae showed the phenotype of OHC loss at P30 (yellow asterisks in Fig. 4*H*). The total length of the missing third-row OHCs along the cochlear duct was 615.4 ± 37.4 μm ($n = 3$) at P1 and 663.5 ± 67.8 μm ($n = 3$) at P30. Moreover, the densities of IHCs at P1 (Myo6⁺/Bcl11b⁻) and P30 (vGlut3⁺) were lower (in basal turn only) in Eh2$^{-/-}$ than Eh2$^{+/+}$ cochleae (Fig. 4 *D'*, *F'*, *I* and *J*). In Eh2$^{-/-}$ mice at P1 and P30, we measured a loss of, respectively, 71.3 ± 1.8 ($n = 3$) and 68.7 ± 2.3 ($n = 3$) OHCs (Fig. 4*K*) and 28.7 ± 3.7 ($n = 3$) and 32.0 ± 6.1 ($n = 3$) IHCs (Fig. 4*L*). However, cochlear lengths at P1 and P30 were
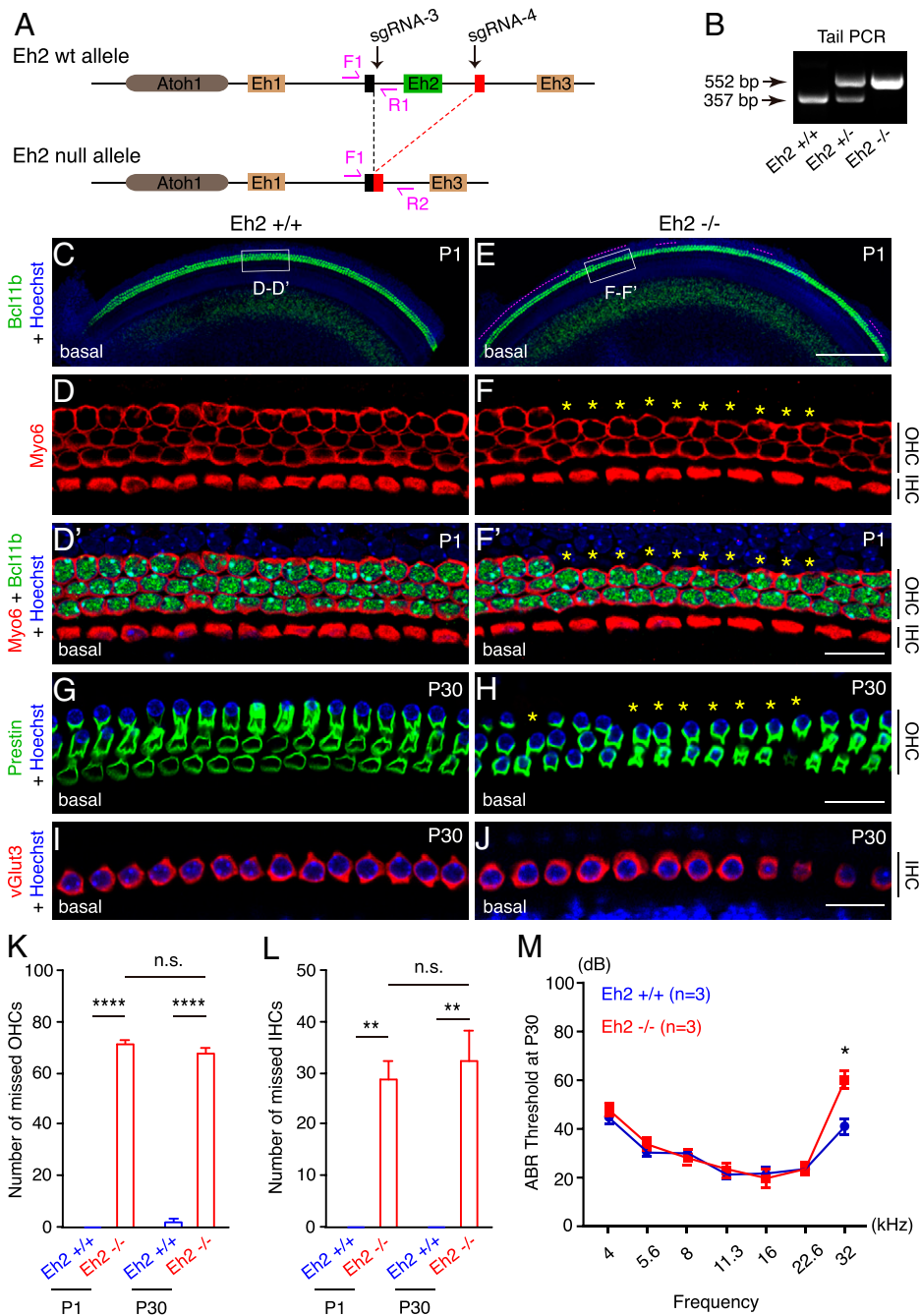

Fig. 4. Deleting Eh2 alone leads to defective cochlear HC development. (*A*) Illustration depicting deletion of Eh2 (~2.5 kb), which lies between the sgRNA-3 and the sgRNA-4 sites. (*B*) Gel image of tail-DNA PCR. WT allele band: 357 bp; Eh2 null-allele band: 552 bp. (*C–F'*) Double labeling for pan-HC marker Myo6 and OHC marker Bcl11b in control Eh2$^{+/+}$ (*C*, *D*, and *D'*) and Eh2$^{-/-}$ (*E*, *F*, and *F'*) mice at P1. Only the Bcl11b channel is shown in *C* and *E*; boxed areas in *C* and *E* are magnified in *D* and *D'* and *F* and *F'*, respectively. The purple line in *E* is the area where third-row OHCs are missing. (*G* and *H*) Labeling for OHC marker Prestin in Eh2$^{+/+}$ (*G*) and Eh2$^{-/-}$ (*H*) mice at P30. Yellow asterisks in *F*, *F'*, and *H* show area where third-row OHCs are missing. (*I* and *J*) Labeling for IHC marker vGlut3 in Eh2$^{+/+}$ (*I*) and Eh2$^{-/-}$ (*J*) mice at P30. (*K* and *L*) Quantification of total missing OHCs (*K*) and IHCs (*L*) in Eh2$^{-/-}$ mice (red) at P1 and P30. In control mice (blue), no OHCs were missing at P1 and very few (2 ± 1.2) were missing at P30. Data are presented as means ± SEM; **$P < 0.01$, ****$P < 0.0001$ (Student's *t* test). (*M*) ABR measurements from Eh2$^{+/+}$ (blue line) and Eh2$^{-/-}$ (red line) mice at P30. Data are presented as means ± SEM. The ABR threshold was not significantly different except at the highest frequency (32 kHz); *$P < 0.05$ (Student's *t* test). Scale bars: 200 μm (*E*), 20 μm (*F'*, *H*, and *J*). Error bar is SEM. n.s.: not significant.

not statistically different between WT mice (5,726.0 ± 78.0 and 5,593.0 ± 162.4 μm) and Eh2$^{-/-}$ mice (5,451.0 ± 62.1 and 5,813.0 ± 155.2 μm).

In accordance with OHCs and IHCs being lost from only the basal turn, ABR measurement revealed that compared to Eh2$^{+/+}$ mice, Eh2$^{-/-}$ mice at P30 exhibited hearing impairment at high frequency (32 kHz) but not at other lower frequencies (Fig. 4M). This type of high-frequency hearing impairment was consistent with basal turn-restricted OHC loss. Notably, we observed no viability problem in Eh2$^{-/-}$ mice. Thus, Eh2 is necessary for proper cochlear HC development, at least in the basal turn of the cochlea.

We also generated a mouse strain harboring a targeted deletion of Eh3; we again used CRISPR-Cas9 and deleted a 907-bp fragment between the sgRNA-5 and the sgRNA-6 sites (*SI Appendix*, Fig. S6 A–D). Relative to control Eh3$^{+/+}$ littermates, Eh3$^{-/-}$ mutants showed no abnormality in HC development at P1 or P30 (*SI Appendix*, Fig. S6 E–F'), and no functional hearing difference was detected at all frequencies between the Eh3$^{+/+}$ and Eh3$^{-/-}$ mice at P30 (*SI Appendix, Fig. S6G*). Moreover, as in Eh2$^{-/-}$ mice, no viability problem was observed in Eh3$^{-/-}$ mice. Thus, similar to Eh1 (Fig. 1), but in contrast to Eh2, Eh3 alone is not necessary for cochlear HC development.

Concurrent Deletion of Eh1 and Eh2 Causes Severe Defects in Cochlear HC Development. The limited cochlear HC phenotypes observed in the three single *Atoh1* enhancer mutants prompted us to hypothesize that Eh1, Eh2, and Eh3 functionally cooperate for *Atoh1* expression (i.e., the enhancers might compensate for each other when one is deleted singly). To test this, we first generated mice harboring deletions in both Eh1 and Eh2. Because Eh1 and Eh2 are closely linked (~62-kb distance), obtaining Eh1$^{-/-}$;Eh2$^{-/-}$ mice by directly breeding Eh1$^{+/-}$ mice with Eh2$^{+/-}$ mice is nearly impossible. Thus, we instead retargeted Eh2 in mice with the Eh1$^{+/-}$ genetic background to obtain double-heterozygous Eh1$^{+/-}$;Eh2$^{+/-}$ mice (*SI Appendix, Fig. S7 A–C*). Myo6 labeling of whole-mount cochlear samples revealed that relative to WT mice (Fig. 5A),

Eh1$^{-/-}$;Eh2$^{-/-}$ mice showed severely impaired cochlear HC development in all turns at P1 (Fig. 5B), which was further confirmed through double labeling for Myo6 and Sox2 in P1 cryosection samples (Fig. 5 C and D). At P1, only 193.0 ± 2.3 Myo6$^+$ HCs were present in Eh1$^{-/-}$;Eh2$^{-/-}$ mice (n = 3), significantly fewer than in control mice (2,882.0 ± 61.5 Myo6$^+$ HCs) (n = 3). The Myo6$^+$ HC number was further decreased to 47.7 ± 5.2 in cochleae of Eh1$^{-/-}$;Eh2$^{-/-}$ mice at P30, which was again considerably lower than in P30 WT cochleae (2,821.0 ± 138.2) (Fig. 5E). Furthermore, as expected, hearing thresholds at all tested frequencies in the ABR assay were significantly higher at P30 in Eh1$^{-/-}$;Eh2$^{-/-}$ mice (n = 3) than in WT mice (n = 3) (Fig. 5F). Notably, similar to Eh1$^{-/-}$ mice, Eh1$^{-/-}$;Eh2$^{-/-}$ mice survived until ~P35. Collectively, our results suggest that Eh1 and Eh2 cooperatively affect cochlear HC development.

Cochlear HCs Respond Differently to Distinct Dual Deletions of *Atoh1* Enhancers. We also generated Eh1$^{-/-}$;Eh3$^{-/-}$ and Eh2$^{-/-}$;Eh3$^{-/-}$ double mutants through gene retargeting (*SI Appendix, Fig. S7 D–I*). Whole-mount Myo6 labeling at P1 revealed that similar to Eh1$^{-/-}$ and Eh3$^{-/-}$ mice, Eh1$^{-/-}$;Eh3$^{-/-}$ mice showed no overt phenotypes (Fig. 6 A–D' and *SI Appendix*, Fig. S8 A–D), which indicates that Eh1 and Eh3 together are less functionally important than Eh2 alone. Moreover, as in Eh2$^{-/-}$ mice (Fig. 6 E and E', and *SI Appendix, Fig. S8E*), OHCs and IHCs were lost in Eh2$^{-/-}$;Eh3$^{-/-}$ mice at P1 (Fig. 6 F and F', and *SI Appendix*, Fig. S8F). We further quantified the missing IHCs and OHCs in these six mouse lines: 1) WT, 2) Eh1$^{-/-}$, 3) Eh3$^{-/-}$, 4) Eh1$^{-/-}$;Eh3$^{-/-}$, 5) Eh2$^{-/-}$, and 6) Eh2$^{-/-}$;Eh3$^{-/-}$ (Fig. 6 G and H). As compared to the number of OHCs absent from Eh2$^{-/-}$ mice (71.3 ± 1.8, basal turn only), substantially more OHCs (179.3 ± 8.3, all turns) were missing in Eh2$^{-/-}$;Eh3$^{-/-}$ mice at P1 (n = 3) (Fig. 6G). Moreover, more IHCs (143.3 ± 8.3, all turns) were lost in Eh2$^{-/-}$;Eh3$^{-/-}$ mice (n = 3) than in Eh2$^{-/-}$ mice (28.7 ± 3.7, basal turn only) (n = 3) at P1 (Fig. 6H). Notably, although IHCs and OHCs were lost in all turns in Eh2$^{-/-}$;Eh3$^{-/-}$ mice, the majority of the loss was in the basal and middle turns (dotted
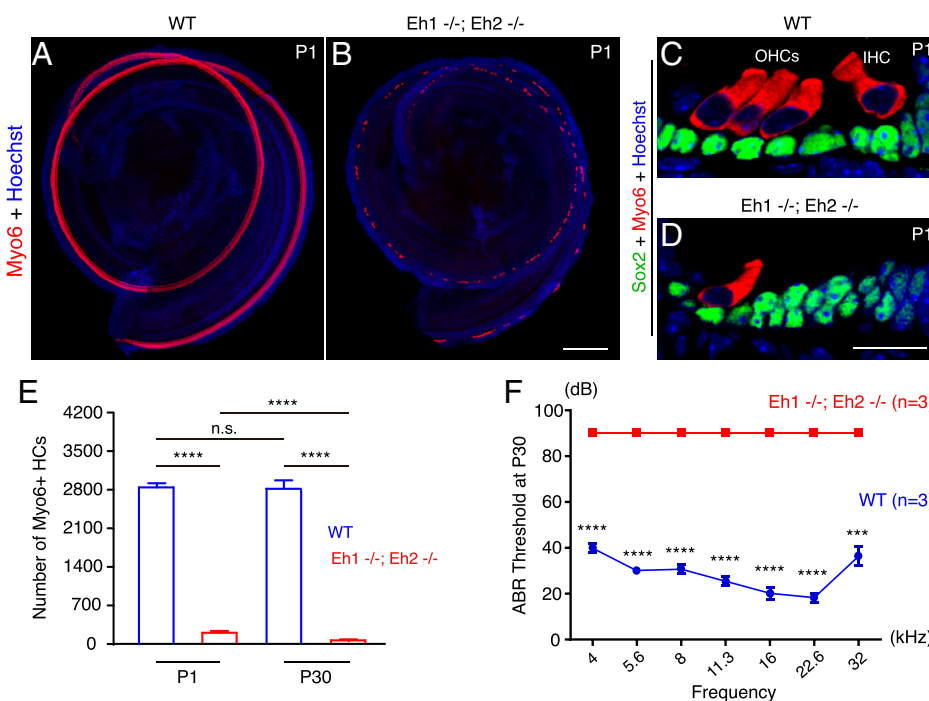

Fig. 5. Concurrent deletion of Eh1 and Eh2 drastically represses cochlear HC production. (A and B) Myo6 labeling of whole-mount cochlear samples from WT (A) and Eh1$^{-/-}$;Eh2$^{-/-}$ (B) mice at P1. (C and D) Double labeling for Myo6 and Sox2 in cryosection cochlear samples from WT (C) and Eh1$^{-/-}$;Eh2$^{-/-}$ (D) mice at P1. Two layers of Sox2$^+$ cells were detected where Myo6$^+$ HCs were missing. (E) Quantification of total Myo6$^+$ HCs in WT control (blue) and Eh1$^{-/-}$;Eh2$^{-/-}$ (red) mice at P1 and P30. Significantly fewer HCs were present in Eh1$^{-/-}$;Eh2$^{-/-}$ mice than in WT mice. Data are presented as means ± SEM; ****P < 0.0001 (Student's t test). (F) ABR measurements from WT mice (blue line) and Eh1$^{-/-}$;Eh2$^{-/-}$ mice (red line) at P30. Eh1$^{-/-}$;Eh2$^{-/-}$ mice exhibited severe hearing impairment at all frequencies. Data are presented as means ± SEM; ***P < 0.001, ****P < 0.0001 (Student's t test). Scale bars: 200 μm (B), 20 μm (D). Error bar is SEM.
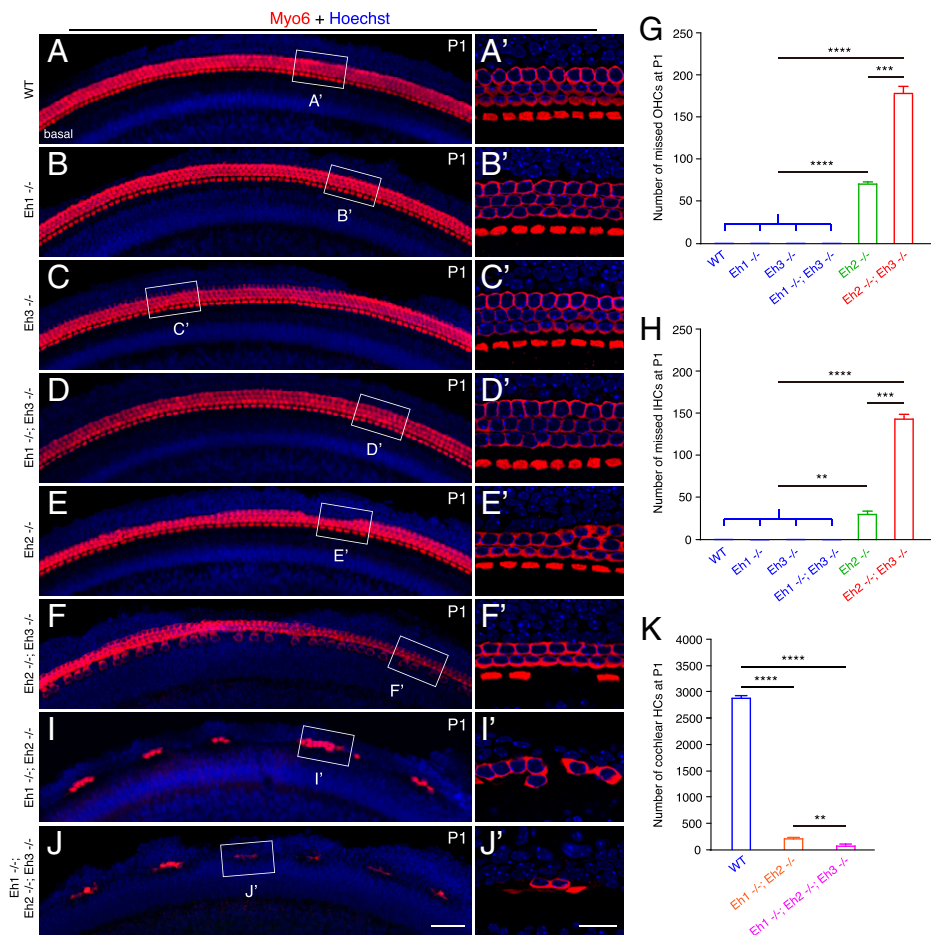
Fig. 6. Parallel comparison of seven mouse models carrying distinct *Atoh1* enhancer mutations. (*A*–*F'*) Myo6 labeling of whole-mount samples from WT mice and five mutant models. Boxed regions in *A*–*F* are magnified in *A'*–*F'*. Relative to WT mice (*A* and *A'*), Eh1$^{-/-}$ (*B* and *B'*), Eh3$^{-/-}$ (*C* and *C'*), and Eh1$^{-/-}$;Eh3$^{-/-}$ (*D* and *D'*) mice exhibited no apparent phenotypes. By contrast, cochlear development phenotypes were detected in Eh2$^{-/-}$ (*E* and *E'*) and Eh2$^{-/-}$; Eh3$^{-/-}$ (*F* and *F'*) mice, with the defect more severe in the double mutant. In these models, IHCs and OHCs can be distinguished by their locations. (*G* and *H*) Quantification of missing OHCs (*G*) and IHCs (*H*) in WT mice and the five mutant models. Data are presented as means ± SEM; **P < 0.01, ***P < 0.001, ****P < 0.0001 (Student's *t* test). (*I*–*J'*) Myo6 labeling of whole-mount samples from two additional mutants. IHCs and OHCs could not be distinguished in Eh1$^{-/-}$;Eh2$^{-/-}$ mice (*I* and *I'*) and Eh1$^{-/-}$;Eh2$^{-/-}$; Eh3$^{-/-}$ mice (*J* and *J'*). (*K*) Quantification of total cochlear HC numbers in WT (blue), Eh1$^{-/-}$;Eh2$^{-/-}$ (orange), and Eh1$^{-/-}$; Eh2$^{-/-}$;Eh3$^{-/-}$ (purple) mice. Data are presented as means ± SEM; **P < 0.01, ****P < 0.0001 (Student's *t* test). Scale bars: 50 μm (*J*), 20 μm (*J'*). Error bar is SEM.

white and yellow lines in *SI Appendix*, Fig. S8*F*). In other words, the degree of HC loss in Eh2$^{-/-}$;Eh3$^{-/-}$ was more than in Eh2$^{-/-}$ but less than in Eh1$^{-/-}$;Eh2$^{-/-}$ mice at P1 (Fig. 6 *E*, *F*, and *I*). Thus, according to the cochlear HC phenotypes in these different enhancer mutants, we roughly rank the functional dependence of *Atoh1* enhancers as Eh2 > Eh1 > Eh3.
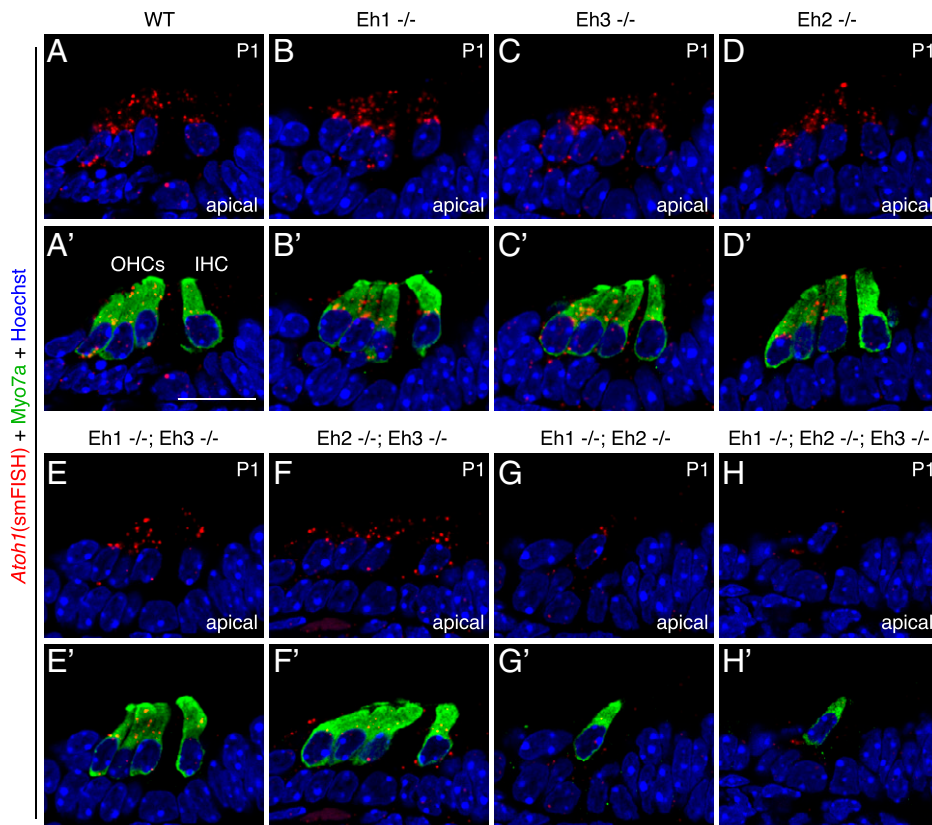
Triple Deletion of Eh1, Eh2, and Eh3 Produces the Most Severe Cochlear HC Development Phenotypes. We next determined whether concurrent deletion of all three *Atoh1* enhancers would completely repress cochlear HC formation. We targeted Eh3 in the Eh1$^{+/-}$;Eh2$^{+/-}$ genetic background to produce Eh1$^{+/-}$;Eh2$^{+/-}$;Eh3$^{+/-}$ triple-heterozygous mice (*SI Appendix*, Fig. S7 *J*–*L*). We predicted that no HCs would be detected in the absence of all three enhancers. However, as in Eh1$^{-/-}$;Eh2$^{-/-}$ mice (Fig. 6 *I* and *I'* and *SI Appendix*, Fig. S8*G*), a few HCs were still present in Eh1$^{-/-}$;Eh2$^{-/-}$;Eh3$^{-/-}$ mice at P1 (Fig. 6 *J* and *J'*, and *SI Appendix*, Fig. S8*H*). We quantified the total number of remaining cochlear HCs in Eh1$^{-/-}$;Eh2$^{-/-}$ (*n* = 3) and Eh1$^{-/-}$;Eh2$^{-/-}$;Eh3$^{-/-}$ mice (*n* = 3), because IHCs and OHCs could not be readily distinguished in these two models (*SI Appendix*, Fig. S8 *G* and *H*). Whereas 2,882.0 ± 61.5 cochlear HCs were present in WT mice at P1, only 193.0 ± 2.3 and 86.0 ± 18.5 cochlear HCs were detected in Eh1$^{-/-}$;Eh2$^{-/-}$ and Eh1$^{-/-}$;Eh2$^{-/-}$;Eh3$^{-/-}$ mice, respectively (Fig. 6*K*). In summary, we rank the four mutants showing HC phenotypes as follows according to the degree of phenotype: 1) Eh1$^{-/-}$; Eh2$^{-/-}$;Eh3$^{-/-}$, 2) Eh1$^{-/-}$;Eh2$^{-/-}$, 3) Eh2$^{-/-}$;Eh3$^{-/-}$, and 4) Eh2$^{-/-}$. Cochlear HC phenotypes were not apparent in the remaining three mutants: 5) Eh1$^{-/-}$, 6) Eh3$^{-/-}$, and 7) Eh1$^{-/-}$;Eh3$^{-/-}$. Notably, in all seven mutants, the total cochlear

length was similar (range: 5,346 to 5,882 μm). These results strongly suggest that all three *Atoh1* enhancers cooperate for *Atoh1* expression and cochlear HC development.

Quantifying *Atoh1* mRNA Levels in Different *Atoh1* Enhancer Mutants. To directly assess the *Atoh1* mRNA level, cochlear samples from all seven mutant mice and WT mice at P1 were subject (in parallel) to single-molecule fluorescence in situ hybridization (smFISH) combined with Myo7a antibody labeling (Fig. 7 *A*–*H*). In this assay, the higher the number of smFISH puncta in cochlear HCs, the higher the level of *Atoh1* mRNA. We selected apical HCs for the comparison because these HCs express *Atoh1* at the highest level (24), and we expected the largest dynamic range of the *Atoh1* mRNA level in these HCs to allow accurate assessment of the differences in distinct mutants.

First, the *Atoh1* mRNA level did not differ markedly among WT, Eh1$^{-/-}$, and Eh3$^{-/-}$ cochlear HCs but was statistically lower in Eh2$^{-/-}$ HCs (Fig. 7*I*). To simply further comparison, we selected the *Atoh1* mRNA level in Eh2$^{-/-}$ as a reference. Second, *Atoh1* mRNA expression in Eh2$^{-/-}$;Eh3$^{-/-}$ HCs was significantly lower than that in Eh2$^{-/-}$ HCs but higher than that in Eh1$^{-/-}$;Eh2$^{-/-}$ HCs (Fig. 7*J*). Third, the lowest levels of *Atoh1* mRNA were similarly detected in Eh1$^{-/-}$;Eh2$^{-/-}$ and Eh1$^{-/-}$;Eh2$^{-/-}$;Eh3$^{-/-}$ HCs (Fig. 7*J*). Collectively, these results show a general negative correlation between *Atoh1* mRNA levels and the degree of defective cochlear HC development.

The Initial HC Fate Specification Is Also Affected in *Atoh1* Enhancer Mutants Showing Defective HC Development at Postnatal Ages. To ascertain whether the initial HC fate specification is defective in the *Atoh1* enhancer mutants that exhibit
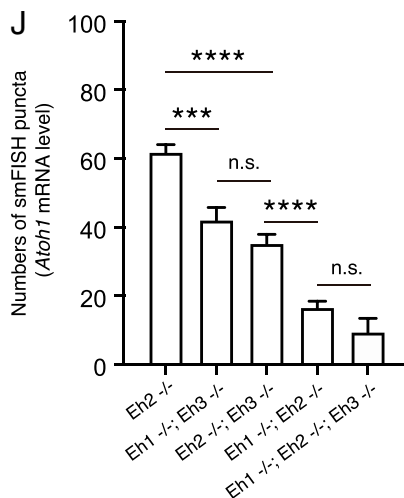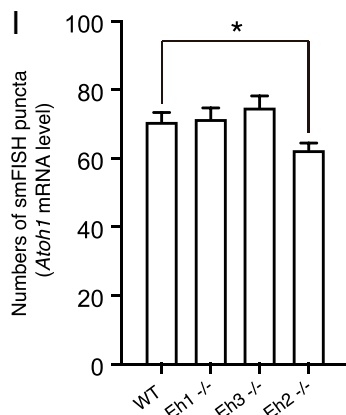
Fig. 7. *Atoh1* mRNA levels are lowest in Eh1$^{-/-}$; Eh2$^{-/-}$ and Eh1$^{-/-}$;Eh2$^{-/-}$;Eh3$^{-/-}$ cochleae. (*A–H'*) Antibody labeling of Myo7a (green) combined with *Atoh1* mRNA (red) smFISH in apical cochleae of WT mice (*A* and *A'*) and seven mutants: Eh1$^{-/-}$ (*B* and *B'*), Eh3$^{-/-}$ (*C* and *C'*), Eh2$^{-/-}$ (*D* and *D'*), Eh1$^{-/-}$;Eh3$^{-/-}$ (*E* and *E'*), Eh2$^{-/-}$;Eh3$^{-/-}$ (*F* and *P*), Eh1$^{-/-}$;Eh2$^{-/-}$ (*G* and *G'*), and Eh1$^{-/-}$;Eh2$^{-/-}$;Eh3$^{-/-}$ (*H* and *H'*). (*I*) Number of smFISH puncta, representing *Atoh1* mRNA level, was lower in Eh2$^{-/-}$ mice than in WT mice, but not Eh1$^{-/-}$ and Eh3$^{-/-}$ mice. Data are presented as means ± SEM; *$P <$ 0.05 (Student's *t* test). (*J*) Quantification of smFISH puncta in five mutants, with Eh2$^{-/-}$ included again as a reference. The *Atoh1* level in Eh1$^{-/-}$; Eh2$^{-/-}$;Eh3$^{-/-}$ mice here appears lower than in Eh1$^{-/-}$;Eh2$^{-/-}$ mice, but the difference was not significant. Data are presented as means ± SEM; ***$P <$ 0.001, ****$P <$ 0.0001 (Student's *t* test). Scale bar: 20 μm (*A'*). Error bar is SEM.

postnatal cochlear HC defects, we examined three mutants (to simplify the analysis) harboring mild, intermediate, and severe cochlear HC defects: 1) Eh2$^{-/-}$, 2) Eh2$^{-/-}$;Eh3$^{-/-}$, and 3) Eh1$^{-/-}$;Eh2$^{-/-}$. Briefly, whole-mount labeling for Myo7a revealed that IHCs and OHCs emerged in the basal turn of WT mice at E16.5 (*SI Appendix*, Fig. S9 *A* and *A'*) and that the three mutants (*n* = 3 each) showed similar HC defects at E16.5 (*SI Appendix*, Fig. S9 *B–D'*) as their counterparts at P1 (Fig. 6). We only focused on the basal turn here because HCs (particularly OHCs) in middle and apical turns had not yet completely emerged at E16.5.

Quantification results showed that the numbers of missing OHCs (29.3 ± 1.8) and IHCs (20.0 ± 3.5) in Eh2$^{-/-}$ basal cochleae (*n* = 3) were significantly lower than the corresponding numbers (116.7 ± 4.4 and 97.3 ± 4.7, respectively) in Eh2$^{-/-}$;Eh3$^{-/-}$ basal cochleae (*n* = 3) (*SI Appendix*, Fig. S9 *E*

and *F*). This agreed with the more severe cochlear defect observed in Eh2$^{-/-}$;Eh3$^{-/-}$ mice than in Eh2$^{-/-}$ mice at P1. Moreover, only 15 ± 6.1 HCs were present in Eh1$^{-/-}$;Eh2$^{-/-}$ basal cochleae (*n* = 3), markedly less than the 792.0 ± 33.6 HCs in WT basal cochleae (*n* = 3) (*SI Appendix*, Fig. S9*G*). These results show that HC fate specification or initial HC differentiation is affected in the three enhancer mutants.

Cerebellum Development Is Defective Only When *Atoh1* Enhancer Mutants Harbor Eh1 Deletion. We next briefly characterized the cerebellum development phenotype in all *Atoh1* mutants, except the triple-homozygous Eh1$^{-/-}$;Eh2$^{-/-}$;Eh3$^{-/-}$ mutant, at P30 (*SI Appendix*, Fig. S10). As in WT mice (*SI Appendix*, Fig. S10 *A* and *A'*), normal cerebellum development was observed in three mutants, Eh2$^{-/-}$, Eh3$^{-/-}$, and Eh2$^{-/-}$; Eh3$^{-/-}$ (*SI Appendix*, Fig. S10 *B–D'*); by contrast, cerebellum

development was severely affected in the other three mutants, $Eh1^{-/-}$, $Eh1^{-/-};Eh2^{-/-}$, and $Eh1^{-/-};Eh3^{-/-}$ (*SI Appendix,* Fig. S10 *E–G'*). Thus, in agreement with the ATAC-seq data (Fig. 2*G*), these results show that Eh1, but not Eh2 or Eh3, is necessary for cerebellum development.

Notably, $Eh1^{-/-}$, $Eh1^{-/-};Eh2^{-/-}$, and $Eh1^{-/-};Eh3^{-/-}$ mice died at ~P35; this was likely due to respiratory failure, because *Atoh1* deletion in the hindbrain retrotrapezoid nucleus leads to severely impaired inspiratory rhythm and pronounced neonatal death (50). Conversely, we observed no survival problem in the mutants that did not include the Eh1 deletion, which suggests that Eh2 and Eh3 are not functionally necessary in hindbrain Atoh1$^+$ neurons.

Atoh1 Binds to All Three *Atoh1* Enhancers in Cochlear HCs In Vivo. Lastly, we investigated whether Atoh1 binds to Eh2 and Eh3, considering that Atoh1 autoregulates its own expression through the Eh1 enhancer (3). In *Atoh1*-EGFP/$^+$ mice, EGFP is fused to the Atoh1 C terminus (40), and an EGFP antibody can recognize the Atoh1-EGFP fusion protein (Fig. 8 *A* and *B*). We performed the CUT&RUN assay on neonatal (P1) fresh cochlear tissues from *Atoh1*-EGFP/$^+$ or *Atoh1*-EGFP/*Atoh1*-EGFP mice (Fig. 8*B*). Cochlear tissues treated with immunoglobulin G (IgG) and EGFP antibody served as the control and experimental groups, respectively.

Peak comparison between IgG-treated (one replicate) and anti-EGFP–treated (two replicates) samples revealed 7,727 high-quality peaks, which were highly reproducible between both replicates (Fig. 8*C* and *SI Appendix,* Fig. S11*A*). Among the 7,727 peaks, 2,019 overlapped with the recently reported Atoh1 CUT&RUN data for E17.5 cochlear HCs (34) (Fig. 8*D*). We identified 1,787 genes that were the nearest to these 2,019 peaks. Gene Ontology (GO) analysis revealed that the top terms were related to inner ear or HC development (Fig. 8*E* and *SI Appendix,* Fig. S11*B*). The entire list of Atoh1 targets in cochlear HCs is reported in Dataset S2. We also compared these Atoh1-binding peaks (2,019) in HCs and the previously reported Atoh1 chromatin immunoprecipitation followed by sequencing (ChIP-seq) data for cerebellar GNPs (38). Unexpectedly, only 10.8% (218/2,019) of the peaks were also detected in cerebellar GNPs, which suggests that Atoh1 binding is highly cell type dependent.

We detected Atoh1-binding peaks in HCs in all three *Atoh1* enhancers, Eh1, Eh2, and Eh3 (Fig. 8*F*), as well as in two other known Atoh1 targets, *Pou4f3* and *Hes6* (*SI Appendix,* Fig. S11 *C* and *D*). Intriguingly, according to the Pou4f3 CUT&RUN data from a recent study (34), Pou4f3 also binds to all three *Atoh1* enhancers, particularly Eh3, which shows a higher peak than Eh1 and Eh2 (*SI Appendix,* Fig. S11*E*). Notably, Eh3 was open in cochlear HCs at P1 but not in the cochlear progenitors at E13.5 (*SI Appendix,* Fig. S11*E*). More importantly, Atoh1 binding to all three enhancers might partly explain why the compensation of Atoh1 at different enhancers could occur.

To predict other potential TFs that also bind to the three Atoh1 enhancers, we annotated Eh1, Eh2, and Eh3 sequences for the 176 representative TF motifs generated from JASPAR 2020 by using the TFmotifView tool (51, 52). Briefly, 89, 109, and 68 representative TF motifs were identified in the Eh1, Eh2, and Eh3 regions, respectively. Notably, 55 TF motifs, including the Six1 and Sox2 motifs, were shared by all three enhancer regions, which agrees with reports that *Atoh1* expression is dependent on Six1 and Sox2 (32, 53, 54). Moreover, 22 TF motifs were present in Eh2 but not in the Eh1 and Eh3 regions. This could explain why Eh2 is the only enhancer

whose single deletion leads to cochlear HC defects. All TF motifs, the 55 shared and the 22 Eh2-specific motifs, are included in Dataset S3. Collectively, our results reveal Atoh1 genomewide targets in neonatal cochlear HCs and demonstrate that Atoh1 binds to Eh1, Eh2, and Eh3, thus providing additional molecular insights into *Atoh1* autoregulation through its enhancers during cochlear HC development.

Discussion

Cochlear HC development is highly dependent on Atoh1. Here, in addition to the previously known Eh1, we identified and validated two unreported *Atoh1* enhancers, Eh2 and Eh3. Furthermore, we annotated potential binding motifs within Eh1, Eh2, and Eh3 for other TFs besides Atoh1, thus identifying 55 shared TF-binding motifs, including Six1- and Sox2-binding motifs (Dataset S3). Moreover, we obtained two lines of evidence indicating that Eh2 is the most functionally important *Atoh1* enhancer for HC development: 1) Eh2 was the only enhancer whose single deletion alone led to cochlear HC defects (Fig. 4) and 2) *Atoh1* mRNA level was decreased in the $Eh2^{-/-}$ model but not the $Eh1^{-/-}$ or $Eh3^{-/-}$ model (Fig. 7*I*). Therefore, we are particularly interested in whether certain unique TF-binding motifs lie within Eh2. The enrichment of Gfi1 and Smad motifs in Eh2 suggests that this *Atoh1* enhancer could be specifically influenced by Gfi1 and the bone morphogenetic protein (BMP) signaling pathway, which play critical roles in cochlear HC development (55, 56). Notably, $Atoh1^{-/-}$ mice die immediately after birth due to inspiratory problems (16, 50), but $Eh1^{-/-};Eh2^{-/-};Eh3^{-/-}$ mice can survive at least until P7. Therefore, besides Eh1, Eh2, and Eh3, other unknown *Atoh1* enhancers likely exist and can drive Atoh1 expression in the brainstem.

In agreement with the notion that Eh1, Eh2, and Eh3 regulate Atoh1 expression in a cooperative manner (Fig. 6), our quantification revealed that the *Atoh1* mRNA level was the lowest in $Eh1^{-/-};Eh2^{-/-}$ or $Eh1^{-/-};Eh2^{-/-};Eh3^{-/-}$ mice, which also exhibited the most severe defects in cochlear HC development (Fig. 7). Overall, we found that the lower the *Atoh1* expression level, the higher the degree of cochlear HC defect. This confirmed the quality of our smFISH quantification results. However, one exception was $Eh1^{-/-};Eh3^{-/-}$: the *Atoh1* mRNA level in $Eh1^{-/-};Eh3^{-/-}$ mice was lower than in $Eh2^{-/-}$ mice (Fig. 7*J*), but $Eh2^{-/-}$ mice, not $Eh1^{-/-};Eh3^{-/-}$ mice, displayed HC defects. Currently, we cannot clearly interpret this finding, but we speculate that concurrent deletion of Eh1 and Eh3 might robustly activate the Atoh1-independent pathway of HC generation, as reported previously (53).

Atoh1 expression patterns and levels are highly dynamic (23–25, 42, 49). First, how is *Atoh1* expression maintained at a low level in cochlear progenitors before E14.5? Failure of initiation of *Atoh1* autoregulation through Eh1 was regarded as one of the key underlying reasons (57). Besides Atoh1, several other TFs, such as Six1 and Sox2, can bind to Eh1 (32, 53, 54). Second, how is the Atoh1 level markedly increased in differentiating cochlear HCs between E14.5 and E17.5? The bivalent status of trimethylation of histone H3 at lysine 27 (H3K27me3)/trimethylation of histone H3 on lysine 4 (H3K4me3) in *Atoh1* disappears, whereas the histone H3 lysine 9 acetylation (H3K9ac) modification (an active mark) is increased in nascent HCs (58), which together contribute to increased efficiency of *Atoh1* transcription. Blocking H3K9ac represses *Atoh1* expression and delays HC differentiation (58). Furthermore, Wnt signaling also affects *Atoh1* expression in nascent HCs, because β-catenin can bind to
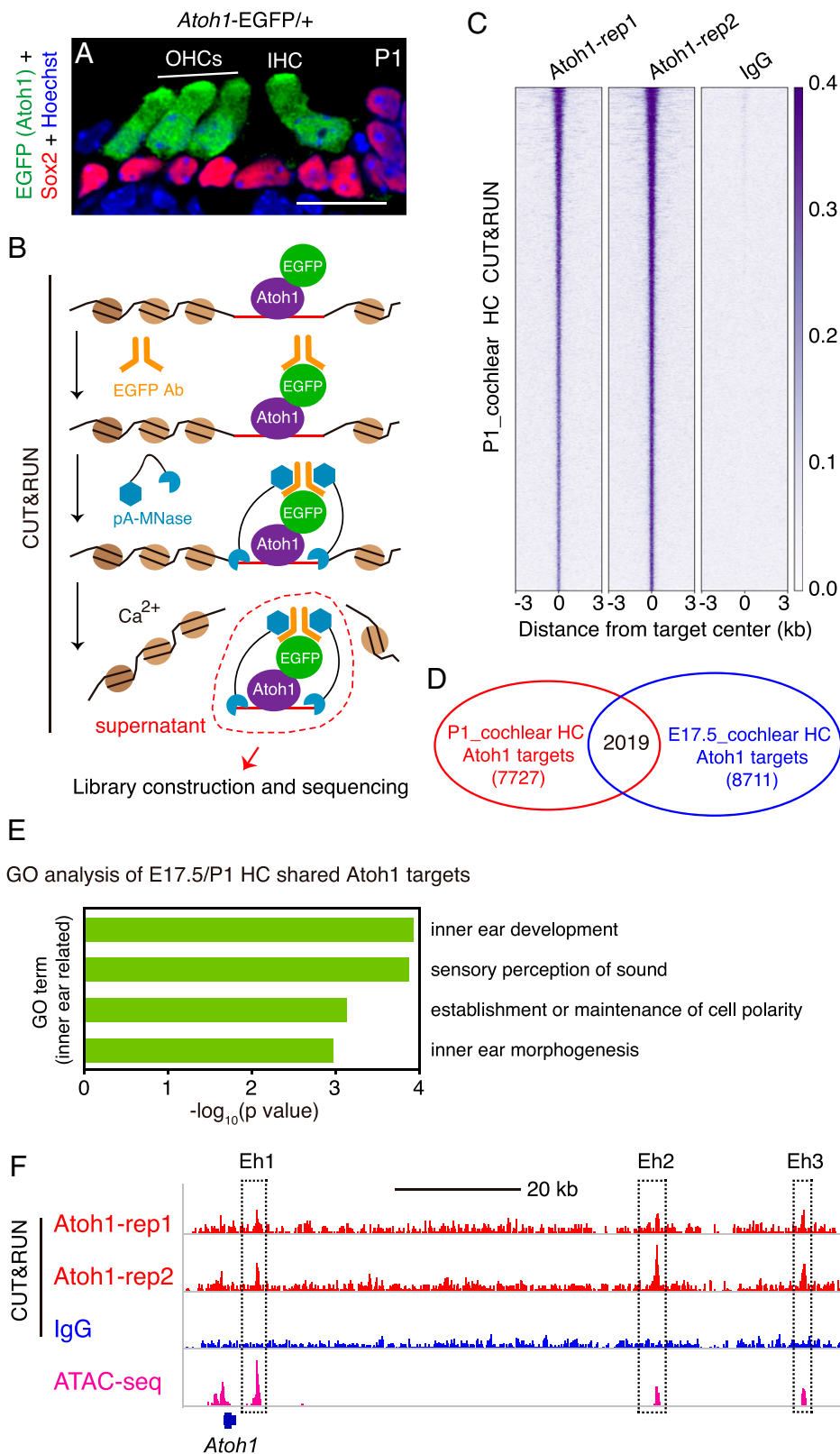
Fig. 8. Genomewide analysis of Atoh1-binding sites by using CUT&RUN. (*A*) Double labeling for EGFP (Atoh1) and Sox2 in a cryo-section cochlear sample from a P1 *Atoh1*-EGFP/⁺ mouse, in which Atoh1 and EGFP are fused. (*B*) Illustration of key steps of the CUT&RUN assay. (*C*) Heatmap showing signals at regions centered at CUT&RUN peaks for EGFP antibody (Atoh1-rep1 and Atoh1-rep2) and IgG (used as control) from the cochlear sensory region of *Atoh1*-EGFP KI mice at P1. (*D*) Diagram depicting overlap of 2019 peaks between our Atoh1-EGFP CUT&RUN results (red) and results from a recent study (34) on E17.5 cochlear HCs (blue). (*E*) GO analysis of genes in which the overlapping peaks are distributed; four GO terms relevant to HC development are presented here as examples, and the entire list of enriched GO terms is presented in *SI Appendix*, Fig. S11*B*. (*F*) Illustration of Atoh1-EGFP CUT&RUN signals obtained with EGFP antibody (red) or IgG (blue), as well as our ATAC-seq data (pink) for P1 cochlear HCs around the *Atoh1* locus. Dotted boxes show EGFP (Atoh1)–binding peaks. Scale bar: 20 μm (*A*).

Eh1 and increase *Atoh1* expression (36). Third, how is the drastic *Atoh1* down-regulation initiated in cochlear HCs between E17.5 and P6? One, the *Atoh1* down-regulation is accompanied by decreased H3K9ac and increased trimethylation of histone H3 on lysine 9 (H3K9me3) in the Eh1 (58). H3K9me3 is a mark associated with transcriptional repression (59). Two, Atoh1 degradation mediated by the E3 ligase Huwe1 might be necessary

for lowering the Atoh1 protein level (60). Three, Atoh1 protein might also undergo a posttranslational modification (61) that could result in the *Atoh1* positive autoregulation no longer being maintained.

Atoh1 is not expressed in postnatal cochlear SCs. However, the contrasting epigenetic states of *Atoh1* or other HC gene enhancers at different ages might determine whether SCs are

able to transdifferentiate into HCs, as revealed by a recent study (33). In cochlear SCs at P1, Eh1 is marked by H3K4me1 but not H3K27ac, which indicates that *Atoh1* is in a poised or primed state; however, this poised state gradually disappears by P6. By reanalyzing previously reported raw data (33), we found that H3K4me1 modification in Eh2 and Eh3, as in Eh1, is also markedly decreased in cochlear SCs at P6. Notably, Eh1 remains in a poised state in utricle SCs at P21, which partly explains why the utricle exhibits a considerably stronger regenerative ability as compared to cochlear tissues (33, 35, 62, 63).

The challenge of adult cochlear SCs to transdifferentiate into HCs suggests that epigenetic barriers are gradually established from perinatal to adult ages. Additional comprehensive and comparative epigenomic analyses of cochlear SCs at distinct postnatal ages should help uncover the epigenetic barriers that prevent transdifferentiation. Eh1 and the two additional enhancers, Eh2 and Eh3, of the master regulator *Atoh1* identified in this study represent a highly suitable target for future investigations seeking to uncover such epigenetic barriers.

Materials and Methods

FACS-Mediated Sorting of Pure Neonatal Cochlear HCs and qPCR Assay. Cochleae were dissected from *Atoh1*-Tdtomato/$^+$ mice at P1; all cochlear HCs were Tdtomato$^+$. Briefly, cochleae were washed in fetal bovine serum (FBS)-free choline chloride solution, incubated in a papain digestion system (Worthington, LK003150) for 15 min at 37 °C, and then incubated in choline chloride solution containing protease and dispase (at a final concentration of 1 mg/mL) at 25 °C for 20 min. All qPCR primers used in this study are listed in Dataset S4.

ATAC-Seq and CUT&RUN. Approximately 500 cochlear HCs or cerebellar GNPs were collected directly into 6 μL of lysis buffer as a biological replicate. ATAC-seq was performed as previously described with minor modifications (39, 64, 65). CUT&RUN was performed according to a previously described protocol with minor modifications (66).

Bioinformatic Analysis. For both ATAC-seq and CUT&RUN analyses, raw reads were first trimmed by using fastp with default parameters (67). The pair-end reads were aligned to the mouse genome (mm10) by using Bowtie2 with the end-to-end parameter (68). Mapped reads were sorted using Samtools (69), and duplicated reads were removed using the Picard MarkDuplicates function (http://broadinstitute.github.io/picard). All sequencing raw data and processed data have been deposited in the Gene Expression Omnibus (GEO) (accession no. GSE181311). The data were also deposited in the gEAR portal (70) (https://umgear.org/p?l=55f7c1cb&g=atoh1).

Generation of *Atoh1*-Tdtomato/$^+$ KI Mice and Distinct *Atoh1* Enhancer-Knockout Mouse Strains. The *Atoh1*-Tdtomato/$^+$ mouse was generated using CRISPR-Cas9–mediated genome editing in a C57BL/6 background. Briefly, *Cas9* mRNA, the sgRNA (against the *Atoh1* locus: 5′-AATGCCCTTCCTAGCGCGCG-3′), and the donor DNA (*SI Appendix*, Fig. S2) were coinjected into one-cell–stage mouse zygotes. Detailed primer sequences are included in Dataset S4. All three *Atoh1* enhancer single-mutant mice were generated using a similar CRISPR-Cas9 approach.

Construction of Eh2-EGFP$^+$ and Eh3-EGFP$^+$ Transgenic Mouse Strains. To produce Eh2-EGFP$^+$ mice, transposase messenger RNA (mRNA) and PiggyBac vector (*SI Appendix*, Fig. S4 A and B) were coinjected into WT one-cell–stage zygotes, after which PCR was performed to screen for founder mice 0 (F0) harboring an insertion of the donor vector in their genomic DNA. A similar strategy was used to generate the Eh3-EGFP$^+$ transgenic mouse strain (*SI Appendix*, Fig. S4 C and D). Detailed DNA sequences of Eh2 (1,027 bp) (*SI Appendix*, Fig. S4A) and Eh3 (761 bp) (*SI Appendix*, Fig. S4C) are included in Dataset S5.

Sample Preparation, Immunohistochemistry, and Cell Counting. Inner ear tissues from E16.5 to P1 mice were directly dissected out and fixed in 4% fresh paraformaldehyde (PFA) overnight at 4 °C. In the case of P30 mice, heart perfusion with 1× phosphate buffered saline (PBS) and then 4% PFA was first performed, and this was followed by a second fixation in 4% PFA overnight at 4 °C. Whole-mount cochlear samples were divided into three parts that were initially scanned at 10× magnification. A line was drawn between OHCs and IHCs to calculate the entire cochlear length.

smFISH Combined with Myo7a Labeling. We performed smFISH as described previously (71). Briefly, inner ear tissues at P1 were dissected out for cryosection. The slices were treated with 10 μg/mL Proteinase K solution at room temperature for 5 min, followed by 4% PFA to stop the Proteinase K reaction, and then incubated with the digoxigenin-labeled *Atoh1* probe; lastly, a tyramide signal amplification kit (catalog NEL753001KT, PerkinElmer) was used to visualize *Atoh1* mRNA. After completing the aforementioned procedure, the slices were incubated with anti-Myo7a antibody overnight at 4 °C.

ABR Measurement. ABR measurements were performed on mice at P30, with the following frequencies being used: 4, 5.6, 8, 11.3, 16, 22.6, and 32 kHz. Detailed assay protocols are described in a previous report (72). Student's *t* test was performed to analyze the statistical difference at each frequency between the control and experimental groups.

Data Availability. ATAC-seq and CUT&RUN data have been deposited in GEO (accession no. GSE181311) (73). All other study data are included in the article and/or supporting information.

Author affiliations: ^{a}State Key Laboratory of Neuroscience, Institute of Neuroscience, Center for Excellence in Brain Science and Intelligence Technology, Chinese Academy of Sciences, Shanghai 200031, China; ^{b}University of Chinese Academy of Sciences, Beijing 100049, China; ^{c}State Key Laboratory of Molecular Developmental Biology, Institute of Genetics and Developmental Biology, Innovative Academy of Seed Design, Chinese Academy of Sciences, Beijing 100101, China; and ^{d}Shanghai Center for Brain Science and Brain-Inspired Intelligence Technology, Shanghai 201210, China

1. M. W. Kelley, Regulation of cell fate in the sensory epithelia of the inner ear. *Nat. Rev. Neurosci.* **7**, 837–849 (2006).
2. D. K. Wu, M. W. Kelley, Molecular mechanisms of inner ear development. *Cold Spring Harb. Perspect. Biol.* **4**, a008409 (2012).
3. A. K. Groves, K. D. Zhang, D. M. Fekete, The genetics of hair cell development and regeneration. *Annu. Rev. Neurosci.* **36**, 361–381 (2013).
4. K. B. Avraham et al., The mouse Snell's waltzer deafness gene encodes an unconventional myosin required for structural integrity of inner ear hair cells. *Nat. Genet.* **11**, 369–375 (1995).
5. R. Grifone, A. Saquet, Z. Xu, D. L. Shi, Expression patterns of Rbm24 in lens, nasal epithelium, and inner ear during mouse embryonic development. *Dev. Dyn.* **247**, 1160–1169 (2018).
6. R. Hertzano et al., Transcription profiling of inner ears from Pou4f3(ddl/ddl) identifies Gfi1 as a target of the Pou4f3 deafness gene. *Hum. Mol. Genet.* **13**, 2143–2153 (2004).
7. G. Wang, C. Li, S. He, Z. Liu, Mosaic CRISPR-stop enables rapid phenotyping of nonsense mutations in essential genes. *Development* **148**, dev196899 (2021).
8. I. Roux et al., Otoferlin, defective in a human deafness form, is essential for exocytosis at the auditory ribbon synapse. *Cell* **127**, 277–289 (2006).
9. J. Ruel et al., Impairment of SLC17A8 encoding vesicular glutamate transporter-3, VGLUT3, underlies nonsyndromic deafness DFNA25 and inner hair cell dysfunction in null mice. *Am. J. Hum. Genet.* **83**, 278–292 (2008).
10. R. P. Seal et al., Sensorineural deafness and seizures in mice lacking vesicular glutamate transporter 3. *Neuron* **57**, 263–275 (2008).
11. J. Zheng et al., Prestin is the motor protein of cochlear outer hair cells. *Nature* **405**, 149–155 (2000).
12. M. C. Liberman et al., Prestin is required for electromotility of the outer hair cell and for the cochlear amplifier. *Nature* **419**, 300–304 (2002).
13. T. Wiwatpanit et al., Trans-differentiation of outer hair cells into inner hair cells in the absence of INSM1. *Nature* **563**, 691–695 (2018).
14. A. Dabdoub et al., Sox2 signaling in prosensory domain specification and subsequent hair cell differentiation in the developing cochlea. *Proc. Natl. Acad. Sci. U.S.A.* **105**, 18396–18401 (2008).

15. A. E. Kiernan et al., Sox2 is required for sensory organ development in the mammalian inner ear. Nature 434, 1031–1035 (2005).
16. N. A. Bermingham et al., Math1: An essential gene for the generation of inner ear hair cells. Science 284, 1837–1841 (1999).
17. J. L. Zheng, W. Q. Gao, Overexpression of Math1 induces robust production of extra hair cells in postnatal rat inner ears. Nat. Neurosci. 3, 580–586 (2000).
18. S. P. Gubbels, D. W. Woessner, J. C. Mitchell, A. J. Ricci, J. V. Brigande, Functional auditory hair cells produced in the mammalian cochlea by in utero gene transfer. Nature 455, 537–541 (2008).
19. M. C. Kelly, Q. Chang, A. Pan, X. Lin, P. Chen, Atoh1 directs the formation of sensory mosaics and induces cell proliferation in the postnatal mammalian cochlea in vivo. J. Neurosci. 32, 6699–6710 (2012).
20. Z. Liu et al., Age-dependent in vivo conversion of mouse cochlear pillar and Deiters' cells to immature hair cells by Atoh1 ectopic expression. J. Neurosci. 32, 6600–6610 (2012).
21. Z. Liu, J. Fang, J. Dearman, L. Zhang, J. Zuo, In vivo generation of immature inner hair cells in neonatal mouse cochleae by ectopic Atoh1 expression. PLoS One 9, e89377 (2014).
22. B. J. Walters et al., In vivo interplay between p27^{Kip1}, GATA3, ATOH1, and POU4F3 converts non-sensory cells to hair cells in adult mice. Cell Rep. 19, 307–320 (2017).
23. V. Matei et al., Smaller inner ear sensory epithelia in Neurog 1 null mice are related to earlier hair cell cycle exit. Dev. Dyn. 234, 633–650 (2005).
24. S. Li et al., Fate-mapping analysis of cochlear cells expressing Atoh1 mRNA via a new Atoh1$^{3*HA-P2A-Cre}$ knockin mouse strain. Dev. Dyn. 7, 1156–1174 (2022).
25. E. C. Driver, L. Sillers, T. M. Coate, M. F. Rose, M. W. Kelley, The Atoh1-lineage gives rise to hair cells and supporting cells within the mammalian cochlea. Dev. Biol. 376, 86–98 (2013).
26. G. A. Wray, The evolutionary significance of cis-regulatory mutations. Nat. Rev. Genet. 8, 206–216 (2007).
27. P. J. Wittkopp, G. Kalay, Cis-regulatory elements: Molecular mechanisms and evolutionary processes underlying divergence. Nat. Rev. Genet. 13, 59–69 (2011).
28. A. W. Helms, A. L. Abney, N. Ben-Arie, H. Y. Zoghbi, J. E. Johnson, Autoregulation and multiple enhancers control Math1 expression in the developing nervous system. Development 127, 1185–1196 (2000).
29. P. Chen, J. E. Johnson, H. Y. Zoghbi, N. Segil, The role of Math1 in inner ear development: Uncoupling the establishment of the sensory primordium from hair cell fate determination. Development 129, 2495–2505 (2002).
30. S. Raft et al., Cross-regulation of Ngn1 and Math1 coordinates the production of neurons and sensory hair cells during inner ear development. Development 134, 4405–4415 (2007).
31. L. M. Chow et al., Inducible Cre recombinase activity in mouse cerebellar granule cell precursors and inner ear hair cells. Dev. Dyn. 235, 2991–2998 (2006).
32. J. Li et al., Dynamic changes in cis-regulatory occupancy by Six1 and its cooperative interactions with distinct cofactors drive lineage-specific gene expression programs during progressive differentiation of the auditory sensory epithelium. Nucleic Acids Res. 48, 2880–2896 (2020).
33. L. Tao et al., Enhancer decommissioning imposes an epigenetic barrier to sensory hair cell regeneration. Dev. Cell 56, 2471–2485.e5 (2021).
34. H. V. Yu et al., POU4F3 pioneer activity enables ATOH1 to drive diverse mechanoreceptor differentiation through a feed-forward epigenetic mechanism. Proc. Natl. Acad. Sci. U.S.A. 118, e2105137118 (2021).
35. H. I. Jen et al., Transcriptomic and epigenetic regulation of hair cell regeneration in the mouse utricle and its potentiation by Atoh1. eLife 8, e44328 (2019).
36. F. Shi, Y. F. Cheng, X. L. Wang, A. S. Edge, Beta-catenin up-regulates Atoh1 expression in neural progenitor cells by interaction with an Atoh1 3′ enhancer. J. Biol. Chem. 285, 392–400 (2010).
37. M. E. Hatten, N. Heintz, Mechanisms of neural patterning and specification in the developing cerebellum. Annu. Rev. Neurosci. 18, 385–408 (1995).
38. T. J. Klisch et al., In vivo Atoh1 targetome reveals how a proneural transcription factor regulates cerebellar development. Proc. Natl. Acad. Sci. U.S.A. 108, 3288–3293 (2011).
39. J. D. Buenrostro, P. G. Giresi, L. C. Zaba, H. Y. Chang, W. J. Greenleaf, Transposition of native chromatin for fast and sensitive epigenomic profiling of open chromatin, DNA-binding proteins and nucleosome position. Nat. Methods 10, 1213–1218 (2013).
40. M. F. Rose et al., Math1 is essential for the development of hindbrain neurons critical for perinatal breathing. Neuron 64, 341–354 (2009).
41. C. Woods, M. Montcouquiol, M. W. Kelley, Math1 regulates development of the sensory epithelium in the mammalian cochlea. Nat. Neurosci. 7, 1310–1318 (2004).
42. H. Yang, X. Xie, M. Deng, X. Chen, L. Gan, Generation and characterization of Atoh1-Cre knock-in mouse line. Genesis 48, 407–413 (2010).
43. T. Cai, M. L. Seymour, H. Zhang, F. A. Pereira, A. K. Groves, Conditional deletion of Atoh1 reveals distinct critical periods for survival and function of hair cells in the organ of Corti. J. Neurosci. 33, 10110–10122 (2013).
44. K. Leto et al., Consensus paper: Cerebellar development. Cerebellum 15, 789–828 (2016).
45. E. Calo, J. Wysocka, Modification of enhancer chromatin: What, how, and why? Mol. Cell 49, 825–837 (2013).
46. E. L. Greer, Y. Shi, Histone methylation: A dynamic mark in health, disease and inheritance. Nat. Rev. Genet. 13, 343–357 (2012).
47. R. Kothary et al., Inducible expression of an hsp68-lacZ hybrid gene in transgenic mice. Development 105, 707–714 (1989).
48. J. Xu et al., Chromatin remodelers and lineage-specific factors interact to target enhancers to establish proneurosensory fate within otic ectoderm. Proc. Natl. Acad. Sci. U.S.A. 118, e2025196118 (2021).
49. T. Tateya et al., Three-dimensional live imaging of Atoh1 reveals the dynamics of hair cell induction and organization in the developing cochlea. Development 146, dev177881 (2019).
50. W. H. Huang et al., Atoh1 governs the migration of postmitotic neurons that shape respiratory effectiveness at birth and chemoresponsiveness in adulthood. Neuron 75, 799–809 (2012).
51. O. Fornes et al., JASPAR 2020: Update of the open-access database of transcription factor binding profiles. Nucleic Acids Res. 48 (D1), D87–D92 (2020).
52. C. Leporcq et al., TFmotifView: A webserver for the visualization of transcription factor motifs in genomic regions. Nucleic Acids Res. 48 (W1), W208–W217 (2020).
53. M. Ahmed et al., Eya1-Six1 interaction is sufficient to induce hair cell fate in the cochlea by activating Atoh1 expression in cooperation with Sox2. Dev. Cell 22, 377–390 (2012).
54. J. Neves, M. Uchikawa, A. Bigas, F. Giraldez, The prosensory function of Sox2 in the chicken inner ear relies on the direct regulation of Atoh1. PLoS One 7, e30871 (2012).
55. M. S. Matern et al., GFI1 functions to repress neuronal gene expression in the developing inner ear hair cells. Development 147, dev186015 (2020).
56. T. Ohyama et al., BMP signaling is necessary for patterning the sensory and nonsensory regions of the developing mammalian cochlea. J. Neurosci. 30, 15044–15051 (2010).
57. Y. Abdolazimi, Z. Stojanova, N. Segil, Selection of cell fate in the organ of Corti involves the integration of Hes/Hey signaling at the Atoh1 promoter. Development 143, 841–850 (2016).
58. Z. P. Stojanova, T. Kwan, N. Segil, Epigenetic regulation of Atoh1 guides hair cell development in the mammalian cochlea. Development 142, 3529–3536 (2015).
59. S. Rea et al., Regulation of chromatin structure by site-specific histone H3 methyltransferases. Nature 406, 593–599 (2000).
60. Y. F. Cheng, M. Tong, A. S. Edge, Destabilization of Atoh1 by E3 ubiquitin Ligase Huwe1 and casein kinase 1 is essential for normal sensory hair cell development. J. Biol. Chem. 291, 21096–21109 (2016).
61. X. J. Quan et al., Post-translational control of the temporal dynamics of transcription factor activity regulates neurogenesis. Cell 164, 460–475 (2016).
62. J. S. Golub et al., Hair cell replacement in adult mouse utricles after targeted ablation of hair cells with diphtheria toxin. J. Neurosci. 32, 15093–15105 (2012).
63. Z. N. Sayyid, T. Wang, L. Chen, S. M. Jones, A. G. Cheng, Atoh1 directs regeneration and functional recovery of the mature mouse vestibular system. Cell Rep. 28, 312–324.e4 (2019).
64. J. Wu et al., The landscape of accessible chromatin in mammalian preimplantation embryos. Nature 534, 652–657 (2016).
65. J. Wu et al., Chromatin analysis in human early development reveals epigenetic transition during ZGA. Nature 557, 256–260 (2018).
66. P. J. Skene, S. Henikoff, An efficient targeted nuclease strategy for high-resolution mapping of DNA binding sites. eLife 6, e21856 (2017).
67. S. Chen, Y. Zhou, Y. Chen, J. Gu, fastp: An ultra-fast all-in-one FASTQ preprocessor. Bioinformatics 34, i884–i890 (2018).
68. B. Langmead, S. L. Salzberg, Fast gapped-read alignment with Bowtie 2. Nat. Methods 9, 357–359 (2012).
69. H. Li et al.; 1000 Genome Project Data Processing Subgroup, The sequence alignment/map format and SAMtools. Bioinformatics 25, 2078–2079 (2009).
70. J. Orvis et al., gEAR: Gene expression analysis resource portal for community-driven, multi-omic data exploration. Nat. Methods 18, 843–844 (2021).
71. X. Tang et al., Bipotent progenitors as embryonic origin of retinal stem cells. J. Cell Biol. 216, 1833–1847 (2017).
72. C. Li et al., Characterizing a novel vGlut3-P2A-iCreER knockin mouse strain in cochlea. Hear. Res. 364, 12–24 (2018).
73. Z. Luo et al., Data from "Three distinct Atoh1 enhancers cooperate for sound receptor hair cell development." Gene Expression Omnibus. http://www.ncbi.nlm.nih.gov/geo/query/acc.cgi?acc=GSE181311. Deposited 2 August 2021.